Published in final edited form as:
Mol Cell. 2009 February 27; 33(4): 528–536. doi:10.1016/j.molcel.2009.01.035.

Alternating access in maltose transporter mediated by rigid-body rotations

Dheeraj Khare[1,4], **Michael L. Oldham**[1,2], **Cedric Orelle**[3], **Amy L. Davidson**[3], and **Jue Chen**[1,2,*]

[1]Department of Biological Sciences, Purdue University, West Lafayette, IN 47907

[2]Howard Hughes Medical Institute, Purdue University, West Lafayette, IN 47907

[3]Department of Chemistry, Purdue University, West Lafayette, IN 47907

Abstract

ATP-binding cassette transporters couple ATP hydrolysis to substrate translocation through an alternating access mechanism, but the nature of the conformational changes in a transport cycle remains elusive. Previously we reported the structure of the maltose transporter $MalFGK_2$ in an outward-facing conformation where the transmembrane (TM) helices outline a substrate-binding pocket open towards the periplasmic surface and ATP is poised for hydrolysis along the closed nucleotide-binding dimer interface. Here we report the structure of the nucleotide-free maltose transporter in which the substrate binding pocket is only accessible from the cytoplasm and the nucleotide-binding interface is open. Comparison of the same transporter crystallized in two different conformations reveals that alternating access involves rigid-body rotations of the TM subdomains that are coupled to the closure and opening of the nucleotide-binding domain interface. The comparison also reveals that point mutations enabling binding-protein independent transport line dynamic interfaces in the TM region.

Introduction

ATP-binding cassette (ABC) transporters are ubiquitous membrane protein complexes that use the energy generated from ATP hydrolysis to transport substances across membranes (Davidson and Maloney, 2007; Higgins, 1992). The types of substrates transported by different members of the ABC superfamily are diverse, ranging from small ions to large polypeptides and polysaccharides (Davidson et al., 2008; Higgins, 1992). Most ABC transporters contain two transmembrane domains (TMDs) that form a pathway for substrates across the membrane and two cytosolic nucleotide-binding domains (NBDs) that bind and hydrolyze ATP. The molecular architecture of ABC transporters has been well established by X-ray crystallography (reviewed in (Hollenstein et al., 2007a; Oldham et al., 2008)). While the folds of the TMDs are diverse, those of the NBDs are highly conserved, containing a RecA-like and a helical subdomains (Oswald et al., 2006). The two NBDs form a head-to-tail dimer with two ATP molecules bound along the interface between the Walker A motif of one subunit and the

*To whom correspondence should be addressed (E-mail: chenjue@purdue.edu).
[4]Present address: Life Sciences Institute, University of Michigan, Ann Arbor, MI 48109

The authors declare no competing financial interests.

signature LSGGQ motif of the second subunit (Hopfner et al., 2000; Smith et al., 2002). The nucleotide-binding dimer interface undergoes cycles of closing to hydrolyze ATP and opening to release products (Chen et al., 2003; Lu et al., 2005). In binding protein dependent importers, the homologous structures of BtuCD (Locher et al., 2002) and HI1470/1 (Pinkett et al., 2007) reveal a central cavity that is open to the periplasm (outward-facing) in one structure and open to the cytoplasm (inward-facing) in the other suggesting that substrate may cross the membrane through an alternating access mechanism (Jardetzky, 1966). The structures of the exporter MsbA in different conformations show large scale re-arrangements of both TMDs and NBDs that could alter the accessibility of a putative substrate-binding site in the TMDs from one side of the membrane to the other (Ward et al., 2007). Because the structures of exporters differ significantly from those of importers, it is not yet clear whether nucleotide-induced conformational changes in the NBDs will trigger the same or different movements of the transmembrane (TM) helices in these two classes of ABC transporters.

Using the maltose transport system as a prototype, we have proposed a model (Chen et al., 2001; Oldham et al., 2007) in which the transporter "rests" with or without ATP bound in an inward-facing conformation with the NBDs open (the resting state). Interactions with the maltose-binding protein (MBP) in the presence of maltose and ATP stimulate the ATPase activity of the transporter by promoting a concerted set of conformational changes in which the NBDs close and the TMDs reorient to receive the substrate from MBP. Previously, we reported the structure of this outward-facing "catalytic intermediate" state using a mutation that prevented ATP hydrolysis (Oldham et al., 2007). Here we describe an inward-facing structure of $MalFGK_2$ that likely represents the resting state. Comparison of the two structures of the same transporter provides insights into the molecular details of an alternating access mechanism for ABC importers, which apparently is distinct from that observed in MsbA (Ward et al., 2007).

Results

Crystallizing the maltose transporter in the resting state

The maltose-binding protein MBP stimulates the ATPase activity of $MalFGK_2$ by stabilizing the transition state for ATP hydrolysis (Chen et al., 2001). Using electron paramagnetic resonance (EPR), we recently showed that the NBD interface is open in the absence of nucleotide and that closure of the NBD interface requires not only the binding of ATP, but also the binding of MBP to the intact transporter (Orelle et al., 2008). Consistent with this data, all of the transporters crystallized without nucleotides display an open NBD interface (Gerber et al., 2008; Hollenstein et al., 2007b; Hvorup et al., 2007; Kadaba et al., 2008; Locher et al., 2002; Pinkett et al., 2007) and the substrate translocation pathway of all, with the exception of BtuCD (Hvorup et al., 2007; Locher et al., 2002), face the cytoplasm.

To obtain a structure of $MalFGK_2$ in the inward-facing conformation, crystallization trials were performed in the absence of nucleotide and MBP. Multiple constructs were tested in an effort to obtain a high resolution structure, though without success, including replacement of large loops with short linkers, deletion of flexible loops, and reduction in surface entropy through amino acid substitution (Goldschmidt et al., 2007). Constructs devoid of the first 1 or 2 TM helices in MalF were also tested since these helices are present in only a subset of maltose transporter homologues (Ehrmann et al., 1998), and, are less ordered in the structure of the outward-facing $MalFGK_2$ transporter (Oldham et al., 2007). The best crystals, obtained using a construct (ΔTM1) lacking residues 2-35, the first TM helix of MalF, diffracted to 4.5 Å along c* and 6.5 Å along a* (Supplementary Fig. 1, Tables 1-2). It has been shown that deletion of residues 2-34 of MalF has little effect on maltose uptake (Ehrmann and Beckwith, 1991). Consistently, our ΔTM1 transporter supports maltose update *in vivo* and displays a MBP-stimulated ATPase activity comparable to that of the wild type (Fig. 1). The structure of ΔTM1

was determined by a combination of selenomethionine (SeMet) MAD phasing and molecular replacement (Supplementary Table 1). The TM helices from the 2.8 Å outward-facing structure were placed individually into the experimental density map (Supplementary Fig. 2), and the registry was verified by the positions of 39 selenium atoms (Supplementary Fig. 3). The structure was refined with strict non-crystallographic symmetry (NCS) and tight secondary structure restraints. The final model does not contain the P2 loop of MalF, as the density for most of this loop is not interpretable (Supplementary Fig. 2).

This new structure (Fig. 2A) is clearly distinct from the outward-facing conformation of MBP-$MalFGK_2$ (Fig. 2B) and displays many of the features anticipated for the resting state transporter. First, the nucleotide-binding interface between the MalK subunits is open rather than closed. Second, TM helices of MalF and MalG are separated in the membrane inner leaflet, generating an aqueous channel that exposes the previously identified maltose-binding site to the cytoplasm. Finally, MalF and MalG are packed together in the outer leaflet, shielding the maltose-binding site from the periplasm. Comparison of the two structures shows that all domain interactions have changed, with the exception of the MalK regulatory domains, where the dimer contacts are maintained. Transition between the two conformations leads to alternation in access for maltose, from one side of the membrane to the other (Fig. 2).

The nature of the conformational changes

To analyze the nature of the conformational changes, each TM subunit is divided into two regions: a core region consisting of the central four helices (TM 2-5 in MalG and TM 4-7 in MalF) and a peripheral region containing helices surrounding the core (Fig. 3A). Similar to the outward-facing structure (Oldham et al., 2007), the core regions of MalF and MalG are related by a pseudo-two-fold symmetry along an axis perpendicular to the membrane bilayer. The helices are arranged in an intertwining configuration in which the peripheral helices of MalG (TM1 and TM6) contact the MalF core and the peripheral helices of MalF pack against the MalG core (Fig. 3A). Superposition of MalG or MalF individually from the two structures (Fig. 3B) shows that the structures of the cores are maintained as rigid-bodies during the switch from inward- to outward-facing conformations (RMSDs < 1.0 Å, Supplementary Table 3). The maltose-binding site, identified in the structure of MBP-$MalFGK_2$ (Oldham et al., 2007), is comprised of 10 residues from 3 different helices of MalF (Fig. 3B). In the inward-facing conformation, access to this binding site from the periplasm is obstructed by a hydrophobic “gate” composed of four loops, each at the bend of a kinked TM helix (Fig. 3C). A similar gating architecture is observed in another ABC transporter $ModB_2C_2A$ (Hollenstein et al., 2007b), even though the primary sequences of the gating regions are quite different. In contrast to the periplasmic gate, the barrier between the maltose-binding site and the cytoplasm in the outward-facing conformation is much larger, with a bundle of four TM helices lying directly beneath the maltose (Fig. 3D).

Using the MalK regulatory domains as a frame of reference, transition from the inward-to the outward-facing structure is achieved by a 22° rotation of the MalF core and a 23° rotation of the MalG core, accompanied by ~4 Å of translation along the rotational axes (Fig. 3E, Supplementary Table 3 and movie 1). The two rotation axes for MalF and MalG are nearly orthogonal, both approximately 45° to the membrane plane. Rotations of both subunits simultaneously open the central pore at the periplasmic side and close it on the cytosolic side. An alternate way to visualize the conformational change is to divide the TM region into two blocks, each consisting of the four core TM helices of one subunit together with the peripheral helices of the other subunit (Fig. 3A). TM1 and TM6 of MalG move together with the MalF core and similarly, TM2, TM3 and TM8 of MalF shift to accommodate movement of the MalG core. Alternating exposure of the substrate-binding site to either side of the membrane is achieved by rotating these two blocks relative to each other.

Conformational changes occurring in the MalK subunits can also be described as rigid-body rotations. In the resting state, the NBDs are separated with the Walker A motif of one monomer facing the LSGGQ loop of the opposite monomer (Fig. 4A). The extent of the separation in this structure, compatible with distance measurements by EPR (Orelle et al., 2008), falls in between those of the semi-open and open structures of isolated MalK crystallized in the absence of nucleotide (Chen et al., 2003). Similar to the "tweezers-like" motion described for isolated MalK (Chen et al., 2003), transition to the closed dimer (Fig. 4B) would involve both a symmetrical rotation of the two entire NBDs by 14° (Fig. 4C and Supplementary Table 3) and an additional rotation of the helical subdomains within each NBD by 12° and 8°. The apparent asymmetry in position of the helical subdomains in the inward-facing conformation may simply be due to the fact that one of them is involved in crystal packing.

Taken together, the transition between the inward- and outward- facing conformations of the maltose transporter can be described as concerted motions of the TM helical cores and the NBDs (Fig. 5 and Supplementary Movies 1-2). Presumably, conformational changes in the ATPase subunits are coupled to movements of the transmembrane subunits via their interface. The connection between the TMD and the NBD is reminiscent of a ball-and-socket joint, with the helix containing the EAA motif (Dassa and Hofnung, 1985), also known as the coupling helix (Hollenstein et al., 2007b), docked into a cleft on the surface of MalK (Fig. 6). The structures of both the surface cleft and the coupling helix are similar among all ABC transporters, suggesting a common mechanism of coupling motions of NBD to the TM domains (Davidson et al., 2008;Hollenstein et al., 2007a). Van der Waals interactions predominate at this interface (Oldham et al., 2007), which may be important to allow movements of the "joint" during structural transitions. When the MalK RecA-like subdomains are superimposed, the coupling helix, along with the TM helical core, rotates about 30° during the outward/inward transition (Fig. 6). The helical subdomain, which makes up one side of the cleft, also rotates to accommodate the motion of the coupling helix (Fig. 6). In the absence of the γ-phosphate of ATP, the relative orientation of the helical subdomain varies significantly among structures of isolated NBDs and intact transporters. When structures of ATP-bound forms are compared, the orientations of the helical subdomains are essentially the same, indicating that the γ-phosphate stabilizes the helical subdomain in one orientation (Davidson and Chen, 2004). Possible roles of the helical subdomain rotation in sensing the γ-phosphate or releasing ADP have been discussed, primarily in the context of isolated NBDs (Davidson and Chen, 2004;Gaudet and Wiley, 2001;Karpowich et al., 2001). The structures of the maltose transporter show that at the NBD/TMD interface, the rotation of the helical subdomain adjusts the "socket", permitting movement of the TMD relative to the NBD without disrupting the tight association of the two subunits.

Binding protein-independent mutants

In binding protein-dependent ABC importers, the binding protein is required to deliver substrate to the transporter and to stimulate ATPase activity (Davidson et al., 1992). However, mutant forms of the maltose transporter have been identified that have gained the ability to hydrolyze ATP in the absence of MBP and maintained specificity for maltose (Covitz et al., 1994; Treptow and Shuman, 1985). The mutations lie at sites of interaction that are altered in the inward/outward transition (Fig 7A). All binding-protein independent (BPI) mutants contain alterations in regions proximal to the periplasmic gate (Covitz et al., 1994; Treptow and Shuman, 1985), including residues 334-338 of MalF (originally designated as the p-site) (Covitz et al., 1994) and L135 of MalG. In the resting state, the p-site interacts with a short helix preceding the MalG P3 (the "scoop") loop (Fig. 7B). In the transition state, this helix is partially released from MalF and the adjacent P3 loop inserts into the MBP substrate-binding site (Oldham et al., 2007). The MBP-independent alleles that do not have a p-site mutation invariably have a mutation in MalG, either L135F or L135H. In the resting state, L135 is within

Van der Waals distance of the MalF P4 loop, and, in the transition state this contact is eliminated as MalG rotates into its new position (Fig. 7C). The two helices containing L135 and the p-site, respectively, are related by the pseudo-two fold symmetry (Fig. 7A). Apparently, alterations in these two regions destabilize contacts between MalF and MalG at the periplasmic surface in the resting state, facilitating the transition to the outward-facing conformation without the assistance of MBP. Most BPI mutants contain a second mutation located elsewhere in the TM subunits (Fig. 7A). The structural roles of these second-site mutations are not always as obvious as the first mutations; however, one of them, V442A of MalF, alters a periplasmic gating residue. In the inward-facing state, V442 forms van der Waals interactions with V230 of MalG (Fig. 7D) and the V442A mutation would destabilize the gate. Possibly the MBP-independent mutations lower the energy barrier between the two conformations, facilitating their inter-conversion without the necessity of the binding protein. In fact, preliminary evidence suggests that some of the BPI mutants may rest in a conformational state that is closer to the transition state than the resting state of the wild-type transporter (Daus et al., 2006; Hall et al., 1997; Mannering et al., 2001).

Discussion

The task of an ABC transporter is to harness the energy of ATP hydrolysis for mechanical work, and this is achieved through conformational coupling within the protein complex. In this study, we directly compare the inward- and outward- facing structures of the maltose transporter and show that alternating access is achieved by concerted rigid-body rotations. In addition, specific features of the transporter likely ensure that maltose is shuttled through the translocation pathway as ATP is hydrolyzed. Structural (Hollenstein et al., 2007b) and biochemical (Austermuhle et al., 2004) data indicate that substrate-loaded binding proteins bind to resting state transporters in the closed conformation. In the structure of the catalytic intermediate state poised for ATP hydrolysis (Oldham et al., 2007), one maltose molecule is occluded in a 6500 $Å^3$ cavity formed between the open MBP and $MalFGK_2$. The local concentration of maltose is approximately 250 mM, high enough to saturate the binding site in the TMDs, which has an estimated affinity of 1 mM, based on the Km for transport in a BPI mutant (Treptow and Shuman, 1985). Because the maltose-binding site in MBP is partially occupied by the scoop loop (Oldham et al., 2007), in this intermediate state maltose would progress from the binding site in MBP to the transmembrane subunits. Following ATP hydrolysis, the outward-facing intermediate is no longer stable and the transporter returns to the resting state. This transition not only alternates access of the binding site (Fig. 2), but also eliminates the occluded state, effectively diluting the maltose concentration and thereby promoting dissociation into the cytoplasm. Higher resolution structures of the inward-facing conformation in the future will address, among other things, whether or not there are local conformational changes accompanying the rigid-body rotations that more actively promote substrate release.

In comparison with other ABC transporters, the substrate translocation pathway observed in the inward-facing maltose transporter is of a similar size to that of the resting state molybdate transporter (Hollenstein et al., 2007b) (Supplementary Fig. 4A), but smaller than those of the methionine (Kadaba et al., 2008) and the molybdate (Gerber et al., 2008) transporters in the "trans-inhibited" state (not shown). As noted before (Kadaba et al., 2008), despite the differences in their sequences and conformational states, the TM core of the maltose, molybdate, and methionine transporters share a common fold (Supplementary Fig. 4B). The fact that the TM cores of the outward-facing and the inward-facing structures are super-imposable suggests that the rigid-body rotations observed in the maltose system and their mechanistic implications of substrate release may well apply to other ABC transporters in which the TM core is conserved.

The nature of the conformational changes in the maltose system differs significantly from those proposed for MsbA (Ward et al., 2007). The transition from the open-apo MsbA to the AMPPNP-bound form involves two motions, gleaned from comparison of three different structures of MsbA. The first is a hinge rotation to bring the NBDs closer, resulting in a closed-apo configuration in which the two Walker A motifs are aligned across the dimer interface. The second motion slides the two NBDs into alignment, bringing Walker A motif of one monomer into proximity to the LSGGQ of the other monomer. The sliding motion, not seen in the maltose transporter, is coupled to the re-orientation of the membrane-spanning helices and consequently the putative substrate-translocation pathway (Ward et al., 2007).

The prevailing model for all active transporters involves alternating access, in which the transporter alternates between an inward-facing conformation with the substrate translocation pathway open to the cytoplasm and an outward-facing conformation with the translocation pathway open to the opposite side (Jardetzky, 1966). As transporters fall into many different families and structural studies have revealed a great diversity in their architecture, the details of how alternating access is achieved may vary. For example, structural comparison of the neurotransmitter transporter LeuT (Singh et al., 2008; Yamashita et al., 2005) and the sodium/galactose symporter vSGLT (Faham et al., 2008) suggests that local rearrangements of several membrane-spanning helices contribute to alternating access (Faham et al., 2008; Singh et al., 2008). In this study, the two structures of the maltose transporter show that alternating access is achieved by global re-arrangements of the transmembrane subunits, a mechanism similar to the “rocker-switch” motion proposed for members of the major facilitator superfamily (Abramson et al., 2003; Huang et al., 2003).

Experimental Procedures

Expression and purification of $MalFGK_2$

Plasmid pFG26 is a variant of pFG23 (Davidson and Nikaido, JBC, 1990) in which sequences downstream of MalF/MalG have been deleted (Supplementary Fig 5). PCR fragment encoding MalF residues 36-514 (ΔTM1) and full-length MalG was cloned into pFG26 at the NcoI and HindIII sites to replace the full-length malFG gene. The resulting plasmid, pFG27, was cotransformed with pKJ, which encodes a C-terminal His-tagged MalK, and pMS421, which encodes $LacI^q$, into the HN741 host strain (Davidson and Nikaido, 1991) for expression of $MalFGK_2$. Protein expression and purification were carried out essentially as described earlier (Oldham et al., 2007). Briefly, the *E. coli* membrane at a protein concentration of 5 mg/ml was resuspended in buffer containing 20 mM Tris pH 8.0, 5mM $MgCl_2$, 10% glycerol, and 0.3% n-Dodecyl-β-D-Maltopyranoside (DDM, Anatrace). Extracted $MalFGK_2$ was purified on cobalt-affinity resin (Clontech) followed by size-exclusion chromatography (Superdex 200, GE Healthcare) in buffer containing 20 mM Tris pH 8.0, 50 mM NaCl and 0.03% n-Undecyl-β-D-Maltopyranoside (UDM, Anatrace). The selenomethionine-labeled transporter was purified similarly except for the addition of 5mM 2-mercaptoethanol and 5mM DTT to the affinity and gel filtration buffers, respectively. Protein was concentrated to 11 mg/ml (Ultra-5 MWCO 100K, Millipore) in the presence of 0.06% UDM prior to crystallization.

ATP hydrolysis assays

$MalFGK_2$ (wild-type or ΔTM1) were reconstituted into proteoliposomes at a lipid-to-protein ratio (mg/mg) of 100:1 as described (Orelle et al., 2008). Briefly, L-α-phosphatidylcholine (Sigma; P5638) at 50 mg/ml in 20 mM Tris-HCl pH 8 was sonicated to clarity and mixed with 1.35% of octyl-β-D-glucopyranoside for 10 minutes at room temperature. Then, protein at 1.3 mg/ml was added to the mixture and the sample was incubated on ice for 10 minutes. Proteoliposomes were obtained by fast dilution (35 fold) into the ATPase reaction mixture containing 50 mM Hepes/KOH pH 8, 10 mM $MgCl_2$, 4 mM phospho-enol pyruvate, 60 μg/

mL pyruvate kinase, 32 μg/mL lactate dehydrogenase, 0.3 Mm NADH, 1.6 mM ATP, in presence or absence of 140 μM maltose and 3 μM MBP. ATP hydrolysis was monitored for 10 minutes at 22°C using a spectrophotometric coupled assay (Scharschmidt et al., 1979).

In vivo maltose transport assay

The plasmids (pFG23, pFG27, or a negative control) were used to transform *E. coli* strain AD110 (Δ(lac pro) supE thi malF::*Tn*10 F'traD36 proAB lacIq ZΔM15). AD110 is a derivative of JM101 with a *Tn*10 insertion inactivating the chromosomal *malF* gene. Cells were then plated on MacConkey agar (Difco) containing 1% maltose and 100 μg/mL ampicillin (Miller, 1972). If plasmid-encoded MalF mutants are functional in transport, colonies will be red after overnight incubation at 37° C.

Crystallization

Crystals were grown by mixing at a 2:1 ratio protein and the reservoir solution containing 11.5% PEG 4000, 0.1M N-(2-Acetamido)iminodiacetic Acid (ADA) pH 6.5, 0.1M NaCl and 0.1M Li_2SO_4. At 20°C in sitting drops, crystals appeared after 24 hours and reached maximum size in about one week. Before data collection, crystals were transferred to a cryosolvent containing the reservoir solution along with 16% ethylene glycol and flash frozen in liquid nitrogen.

Structure determination

X-ray diffraction data were collected at the Advanced Photon Source GM/CA CAT at 100 K. Diffraction images were processed and scaled with HKL2000 (Otwinowski and Minor, 1997). The structures of isolated MalK dimer (PDB accession numbers 1Q1E or 1Q1B) were used as search models for molecular replacement. Although both models produced clear solutions, the resulting maps for the transmembrane subunits were difficult to interpret. The molecular replacement phase was used to calculate an anomalous-difference Fourier map, using diffraction data measured from selenomethionine-substituted $MalFGK_2$ at the selenium peak wavelength (Supplementary Table 1). Contoured at 2.5σ, 77 out of 90 selenium positions in the asymmetric unit were located. The selenium substructure was refined in SHARP (Abrahams and Leslie, 1996) and the experimental phase was improved by density modification and phase extension to 4.5 Å. The transmembrane helices defined in the 2.8 Å structure of MBP-$MalFGK_2$ (PDB accession number 2R6G) were placed into the experimental density map manually, guided by the selenium positions. The atomic model and the experimental phase were improved by an iterative loop involving model-building, refinement of selenium substructure, phase combination, and model refinement. Model was built in COOT (Emsley and Cowtan, 2004) and refined in CNS (Brunger, 2007) using the MLHL target with strict non-crystallographic symmetry restraints. Distance restraints to maintain main-chain hydrogen bonds in α-helices and β-sheets obtained from the WHAT IF server (Hooft et al., 1996) were imposed during the refinement.

Figure preparation

Domain movements were analyzed by DynDom (Hayward and Berendsen, 1998). All figures were prepared using the program PyMOL (DeLano Scientific, CA).

Supplementary Material

Refer to Web version on PubMed Central for supplementary material.

Acknowledgments

We thank the staff at the Advanced Photon Source GM/CA CAT for assistance with data collection. We also thank Dr. Paul Paukstelis for help with distance restraints, Frances J. Alvarez for performing the MacConkey plate assay, Drs. Barbara Golden and Dinesh Yernool for discussions, and the Purdue Cancer Center for X-ray and DNA sequencing facilities. This work was supported by NIH grants (J.C. and A.L.D.) and a postdoctoral fellowship from American Heart Association (M.L.O). Coordinates and structure factors have been deposited in the Protein Data Bank under accession number 3FH6.

References

Abrahams JP, Leslie AG. Methods used in the structure determination of bovine mitochondrial F1 ATPase. Acta Crystallogr D Biol Crystallogr 1996;52:30–42. [PubMed: 15299723]

Abramson J, Smirnova I, Kasho V, Verner G, Kaback HR, Iwata S. Structure and mechanism of the lactose permease of Escherichia coli. Science 2003;301:610–615. [PubMed: 12893935]

Austermuhle MI, Hall JA, Klug CS, Davidson AL. Maltose-binding protein is open in the catalytic transition state for ATP hydrolysis during maltose transport. J Biol Chem 2004;279:28243–28250. [PubMed: 15117946]

Brunger AT. Version 1.2 of the Crystallography and NMR system. Nat Protoc 2007;2:2728–2733. [PubMed: 18007608]

Chen J, Lu G, Lin J, Davidson AL, Quiocho FA. A tweezers-like motion of the ATP-binding cassette dimer in an ABC transport cycle. Mol Cell 2003;12:651–661. [PubMed: 14527411]

Chen J, Sharma S, Quiocho FA, Davidson AL. Trapping the transition state of an ATP-binding-cassette transporter: Evidence for a concerted mechanism of maltose transport. Proc Natl Acad Sci U S A 2001;98:1525–1530. [PubMed: 11171984]

Covitz K-MY, Panagiotidis CH, Reyes M, Treptow NA, Shuman HA. Mutations that alter the transmembrane signalling pathway in an ATP binding cassette (ABC) transporter. EMBO J 1994;13:1752–1759. [PubMed: 8157012]

Dassa E, Hofnung M. Sequence of gene *malG* in *E. coli* K12: homologies between integral membrane components from binding protein-dependent transport systems. EMBO J 1985;4:2287–2293. [PubMed: 3000770]

Daus ML, Landmesser H, Schlosser A, Muller P, Herrmann A, Schneider E. ATP induces conformational changes of periplasmic loop regions of the maltose ATP-binding cassette transporter. J Biol Chem 2006;281:3856–3865. [PubMed: 16352608]

Davidson AL, Chen J. ATP-binding cassette transporters in bacteria. Annu Rev Biochem 2004;73:241–268. [PubMed: 15189142]

Davidson AL, Dassa E, Orelle C, Chen J. Structure, function, and evolution of bacterial ATP-binding cassette systems. Microbiol Mol Biol Rev 2008;72:317–364. [PubMed: 18535149]

Davidson AL, Maloney PC. ABC transporters: how small machines do a big job. Trends Microbiol 2007;15:448–455. [PubMed: 17920277]

Davidson AL, Nikaido H. Purification and characterization of the membrane-associated components of the maltose transport system from *Escherichia coli*. J Biol Chem 1991;266:8946–8951. [PubMed: 2026607]

Davidson AL, Shuman HA, Nikaido H. Mechanism of maltose transport in Escherichia coli: Transmembrane signalling by periplasmic binding proteins. Proceedings of the National Academy of Sciences U S A 1992;89:2360–2364.

Ehrmann M, Beckwith J. Proper insertion of a complex membrane protein in the absence of its amino-terminal export signal. J Biol Chem 1991;266:16530–16533. [PubMed: 1885584]

Ehrmann M, Ehrle R, Hofmann E, Boos W, Schlosser A. The ABC maltose transporter. Mol Microbiol 1998;29:685–694. [PubMed: 9723909]

Emsley P, Cowtan K. Coot: model-building tools for molecular graphics. Acta Crystallogr D Biol Crystallogr 2004;60:2126–2132. [PubMed: 15572765]

Faham S, Watanabe A, Besserer GM, Cascio D, Specht A, Hirayama BA, Wright EM, Abramson J. The crystal structure of a sodium galactose transporter reveals mechanistic insights into Na+/sugar symport. Science 2008;321:810–814. [PubMed: 18599740]

Gaudet R, Wiley DC. Structure of the ABC ATPase domain of human TAP1, the transporter associated with antigen processing. EMBO J 2001;20:4964–4972. [PubMed: 11532960]

Gerber S, Comellas-Bigler M, Goetz BA, Locher KP. Structural basis of trans-inhibition in a molybdate/tungstate ABC transporter. Science 2008;321:246–250. [PubMed: 18511655]

Goldschmidt L, Cooper DR, Derewenda ZS, Eisenberg D. Toward rational protein crystallization: A Web server for the design of crystallizable protein variants. Protein Sci 2007;16:1569–1576. [PubMed: 17656576]

Hall JA, Thorgeirsson TE, Liu J, Shin YK, Nikaido H. Two modes of ligand binding in maltose-binding protein of Escherichia coli. Electron paramagnetic resonance study of ligand-induced global conformational changes by site-directed spin labeling. J Biol Chem 1997;272:17610–17614. [PubMed: 9211909]

Hayward S, Berendsen HJ. Systematic analysis of domain motions in proteins from conformational change: new results on citrate synthase and T4 lysozyme. Proteins 1998;30:144–154. [PubMed: 9489922]

Higgins CF. ABC transporters: from microorganisms to man. Annu Rev Cell Biol 1992;8:67–113. [PubMed: 1282354]

Hollenstein K, Dawson RJ, Locher KP. Structure and mechanism of ABC transporter proteins. Curr Opin Struct Biol 2007a;17:412–418. [PubMed: 17723295]

Hollenstein K, Frei DC, Locher KP. Structure of an ABC transporter in complex with its binding protein. Nature 2007b;446:213–216. [PubMed: 17322901]

Hooft RW, Sander C, Vriend G. Positioning hydrogen atoms by optimizing hydrogen-bond networks in protein structures. Proteins 1996;26:363–376. [PubMed: 8990493]

Hopfner KP, Karcher A, Shin DS, Craig L, Arthur LM, Carney JP, Tainer JA. Structural biology of Rad50 ATPase: ATP-driven conformational control in DNA double-strand break repair and the ABC-ATPase superfamily. Cell 2000;101:789–800. [PubMed: 10892749]

Huang Y, Lemieux MJ, Song J, Auer M, Wang DN. Structure and mechanism of the glycerol-3-phosphate transporter from Escherichia coli. Science 2003;301:616–620. [PubMed: 12893936]

Hvorup RN, Goetz BA, Niederer M, Hollenstein K, Perozo E, Locher KP. Asymmetry in the Structure of the ABC Transporter Binding Protein Complex BtuCD-BtuF. Science. 2007

Jardetzky O. Simple allosteric model for membrane pumps. Nature 1966;211:969–970. [PubMed: 5968307]

Kadaba NS, Kaiser JT, Johnson E, Lee A, Rees DC. The high-affinity E. coli methionine ABC transporter: structure and allosteric regulation. Science 2008;321:250–253. [PubMed: 18621668]

Karpowich N, Martsinkevich O, Millen L, Yuan Y, Dai PL, MacVey K, Thomas PJ, Hunt JF. Crystal structures of the MJ1267 ATP binding cassette reveal an induced-fit effect at the ATPase active site of an ABC transporter. Structure 2001;9:571–586. [PubMed: 11470432]

Locher KP, Lee AT, Rees DC. The E. coli BtuCD structure: a framework for ABC transporter architecture and mechanism. Science 2002;296:1091–1098. [PubMed: 12004122]

Lu G, Westbrooks JM, Davidson AL, Chen J. ATP hydrolysis is required to reset the ATP-binding cassette dimer into the resting-state conformation. Proc Natl Acad Sci U S A 2005;102:17969–17974. [PubMed: 16326809]

Mannering DE, Sharma S, Davidson AL. Demonstration of conformational changes associated with activation of the maltose transport complex. J Biol Chem 2001;376:12362–12368. [PubMed: 11150310]

Miller, JH. Experiments in Molecular Genetics. Cold Spring Harbor, NY: Cold Spring Harbor Laboratory; 1972.

Oldham ML, Davidson AL, Chen J. Structural insights into ABC transporter mechanism. Curr Opin Struct Biol 2008;18:726–733. [PubMed: 18948194]

Oldham ML, Khare D, Quiocho FA, Davidson AL, Chen J. Crystal structure of a catalytic intermediate of the maltose transporter. Nature 2007;450:515–521. [PubMed: 18033289]

Orelle C, Ayvaz T, Everly RM, Klug CS, Davidson AL. Both maltose-binding protein and ATP are required for nucleotide-binding domain closure in the intact maltose ABC transporter. Proc Natl Acad Sci U S A 2008;105:12837–12842. [PubMed: 18725638]

Oswald C, Holland IB, Schmitt L. The motor domains of ABC-transporters. What can structures tell us? Naunyn Schmiedebergs Arch Pharmacol 2006;372:385–399. [PubMed: 16541253]

Otwinowski Z, Minor W. Processing of X-ray diffraction data collected in oscillation mode. Meth Enzymol 1997;276:307–326.

Pinkett HW, Lee AT, Lum P, Locher KP, Rees DC. An inward-facing conformation of a putative metal-chelate-type ABC transporter. Science 2007;315:373–377. [PubMed: 17158291]

Scharschmidt BF, Keefe EB, Blankenship NM, Ockner RK. Validation of a recording spectrophotometric method for measurement of membrane-associated Mg- and NaK-ATPase activity. J Lab Clin Med 1979;93:790–799. [PubMed: 219124]

Singh SK, Piscitelli CL, Yamashita A, Gouaux E. A competitive inhibitor traps LeuT in an open-to-out conformation. Science 2008;322:1655–1661. [PubMed: 19074341]

Smith PC, Karpowich N, Millen L, Moody JE, Rosen J, Thomas PJ, Hunt JF. ATP binding to the motor domain from an ABC transporter drives formation of a nucleotide sandwich dimer. Mol Cell 2002;10:139–149. [PubMed: 12150914]

Treptow NA, Shuman HA. Genetic evidence for substrate and periplasmic-binding-protein recognition by the MalF and MalG proteins, cytoplasmic membrane components of the *Escherichia coli* maltose transport system. J Bacteriol 1985;163:654–660. [PubMed: 3894331]

Ward A, Reyes CL, Yu J, Roth CB, Chang G. Flexibility in the ABC transporter MsbA: Alternating access with a twist. Proc Natl Acad Sci U S A 2007;104:19005–19010. [PubMed: 18024585]

Yamashita A, Singh SK, Kawate T, Jin Y, Gouaux E. Crystal structure of a bacterial homologue of Na +/Cl--dependent neurotransmitter transporters. Nature 2005;437:215–223. [PubMed: 16041361]

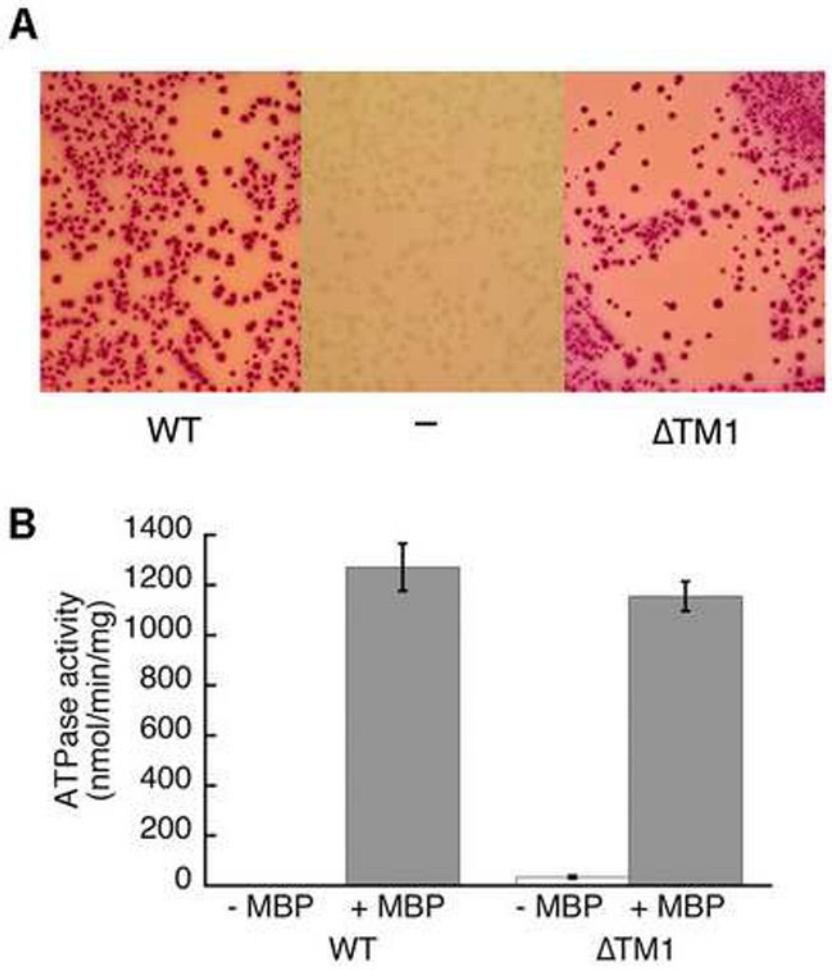

Figure 1. Functional Assay of the ΔTM1 construct

(A) Maltose transport was analyzed on MacConkey plates in a strain carrying a *Tn*10 insertion in *malF* (see Experimental Procedures). A red color indicates that maltose is transported. An empty vector was used as a negative control. (B) MBP-stimulated ATPase activity of purified $MalFGK_2$ reconstituted into proteoliposomes (see Experimental Procedures). Each bar shows the average and standard deviation of 3 to 4 independent measurements.

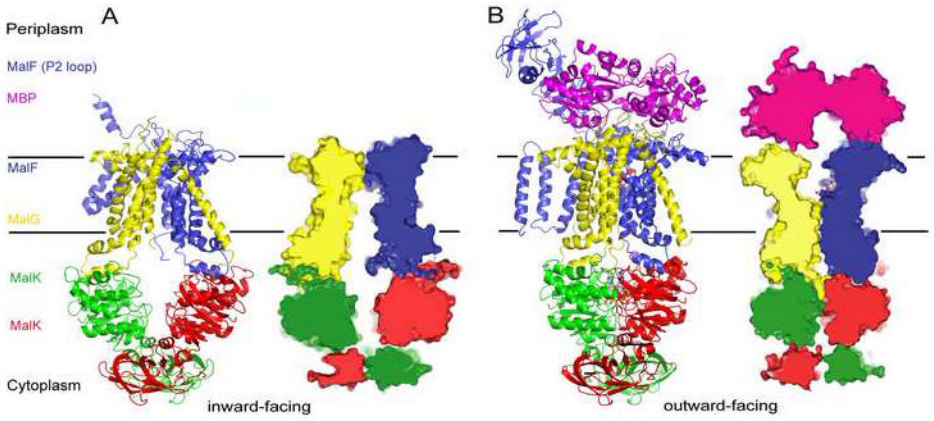

Figure 2. Alternating access in the maltose transporter

Ribbon diagram (left) and a 12-Å slab view (right) of the maltose transporter in (A) the inward-facing, resting state conformation and (B) the outward-facing, catalytic intermediate conformation (Oldham et al., 2007). The maltose and ATP are shown in CPK and ball-and-stick models, respectively.

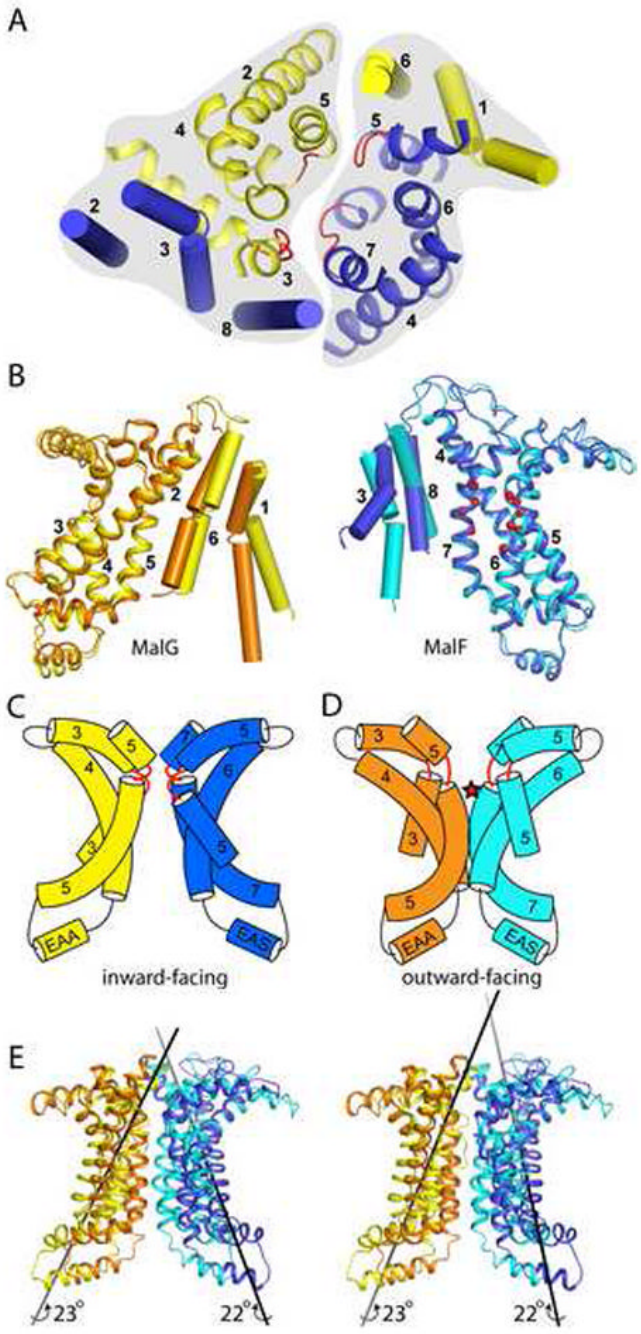

Figure 3. Conformational changes in the transmembrane subunits

(A) The architecture of MalG (yellow) and MalF (blue) in the inward-facing conformation, viewed along the membrane normal from the cytoplasm. Helices in the core and peripheral regions are shown in ribbon and cylinder representations, respectively. Residues constituting the periplasmic gate are shown in red. The two gray masks specify helices that move in concert during the structural transition. (B) Superposition of MalG (left) and MalF (right) as they occur in the resting and transition-state conformations. Residues involved in maltose binding are specified by red dots. (C) Cartoon showing the translocation pathway in the resting and (D) the transition states. The location of maltose in the outward-facing conformation is indicated by a red star. Gating loops are shown in red. The two coupling helices, also known as EAA

loops of MalG and MalF, are labeled by “EAA” and “EAS”, respectively, based on their sequence. (E) Stereoview of the TM cores, the inward- and outward facing structures are superimposed based on the MalK regulatory domains. The grey lines indicate the two rotation axes relative to the regulatory domains. Color codes: MalG resting state, yellow, transition state, orange; MalF resting state, blue, transition state, cyan.

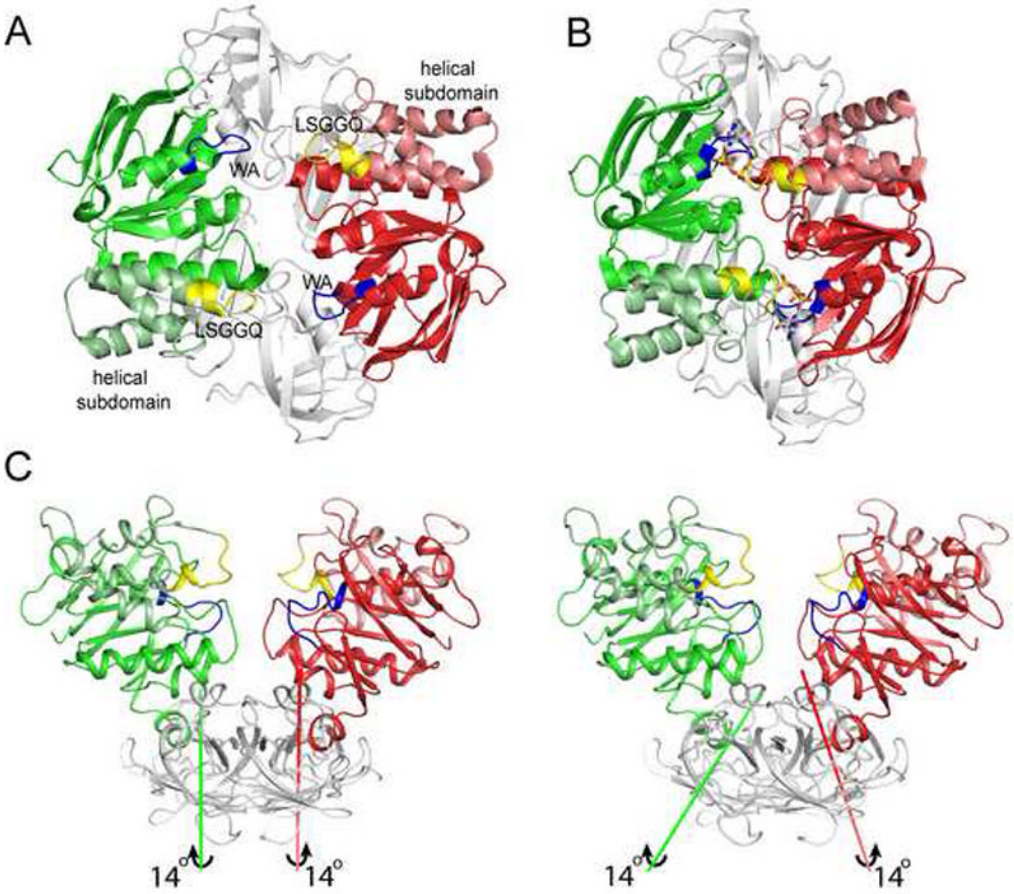

Figure 4. Conformational changes in the MalK subunits

Ribbon diagram of the MalK (A) open dimer in the inward-facing structure and (B) closed dimer in the outward-facing structure. The two NBDs are colored in green and red and the regulatory domains are colored in grey. The helical subdomains are indicated and colored in light green or red. The Walker A (WA) and the LSGGQ motifs are colored in blue and yellow, respectively. ATP is shown in stick models. (C) Stereo-diagram of MalK in the resting state. Using the regulatory domains (grey) as the frame of reference, rotations of the two NBDs (green and red) leading to the closed dimer are indicated.

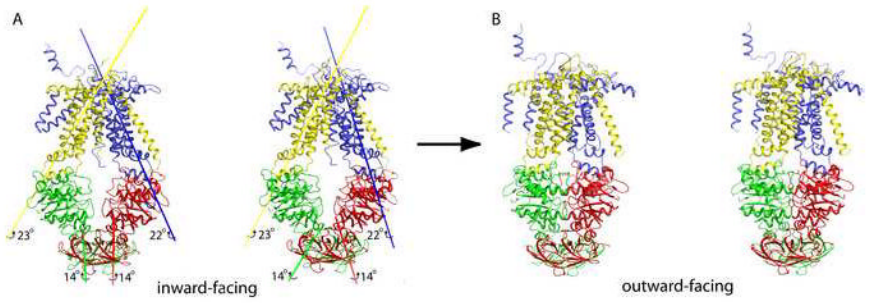

Figure 5. Rigid body rotations that mediate alternating access

(A) Stereoview of the maltose transporter in the inward-facing conformation with rotation axes indicated (color codes are consistent with those of the protein subunits). (B) Stereoview of the outward-facing structure (regions that are not observed in the inward-facing structure are omitted). The rotation axes of the helical subdomains are not shown.

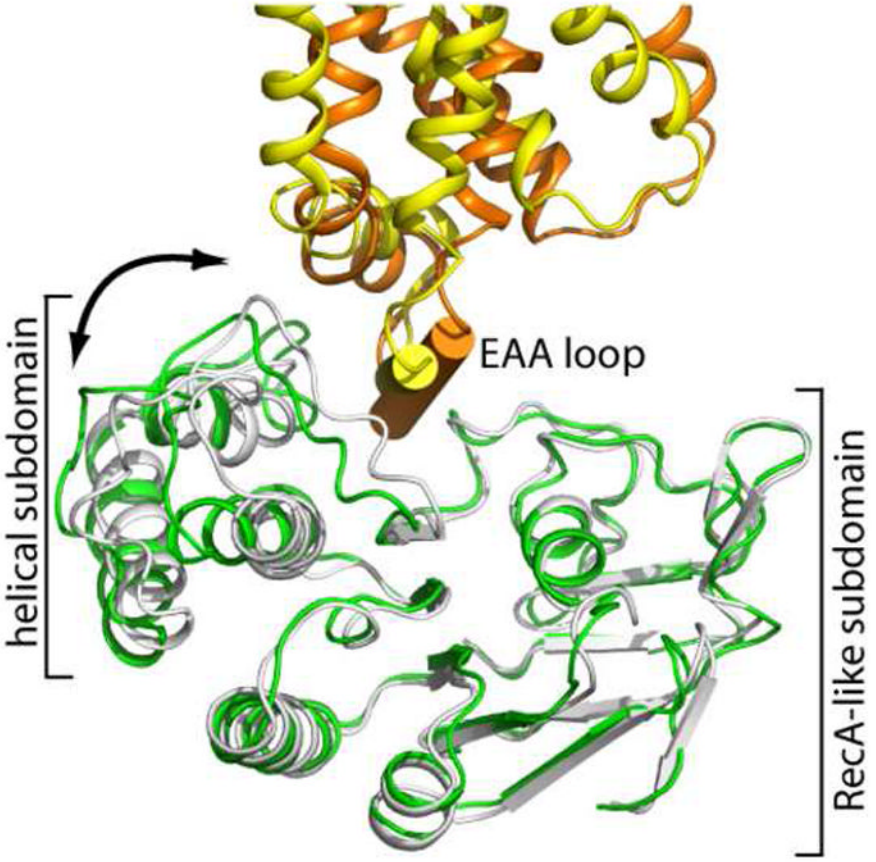

Figure 6. Conformational change at the MalK/TMD interface

The structures are superpositioned based on the RecA-like subdomains of MalK. The NBDs of MalK from the inward- and outward-facing structures are shown in green and grey, respectively. MalG is rendered in yellow (resting state) and orange (transition state). The coupling helix is labeled as “EAA loop”.

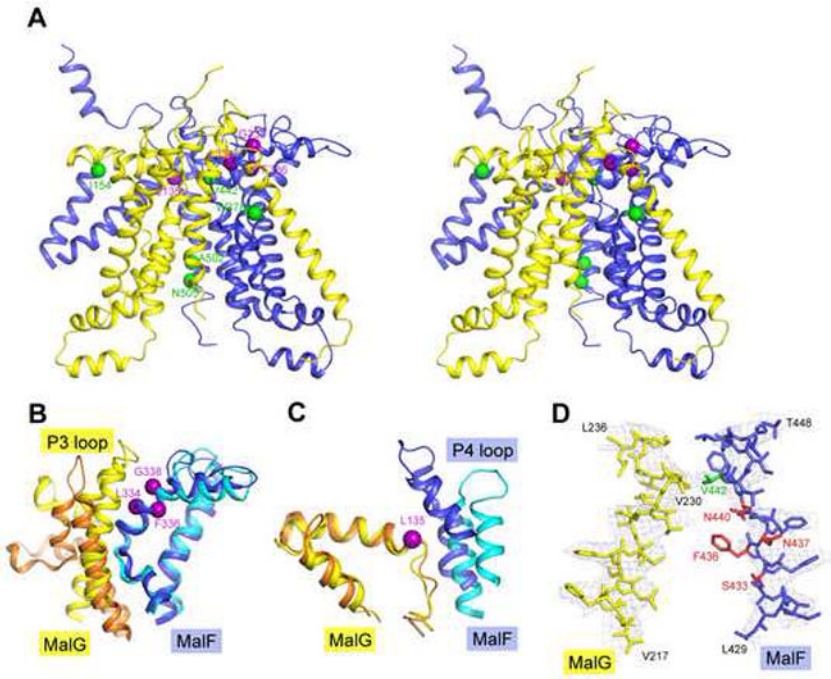

Figure 7. The binding-protein independent mutants

(A) Stereoview of MalFG in the resting state showing the positions of mutations that enable transport without MBP (Covitz et al., 1994). The p-site mutations (L334W, F336L, and G338R) of MalF and MalG L135F are shown in magenta. The second-site mutations (MalF W378C, V442A, A502V, N505I, and MalG I154S) are shown in green. (B) A close-up view of the p-site interaction with MalG. (C) Interactions of MalG L135 and MalF. (D) Contacts between MalF V442 and MalG V230, together with σ_A-weighted phased-combined $2F_o$-F_c electron density maps with a B-factor sharpening factor of -140 $Å^2$ contoured at 1 σ. Maltose-binding residues are shown in red. Color identification is as in Fig 3.